Acta Crystallographica Section B
Structural Science
ISSN 0108-7681

Incommensurately modulated ordering of tetrahedral chains in $Ca_2Fe_2O_5$ at elevated temperatures

Hannes Krüger* and Volker Kahlenberg

Institut für Mineralogie und Petrographie der Leopold-Franzens-Universität, A-6020 Innsbruck, Austria

Correspondence e-mail: hannes.krueger@uibk.ac.at

Received 2 June 2005
Accepted 18 August 2005

The basic building units of brownmillerite-type $A_2B_2O_5$ structures are perovskite-like layers of corner-sharing BO_6 octahedra and *zweier* single chains of BO_4 tetrahedra. A three-dimensional framework is formed by alternate stacking of octahedral layers and sheets of tetrahedral chains. The compound $Ca_2Fe_2O_5$ is known to have *Pnma* symmetry at ambient conditions. The space group *Imma* was reported to be evident above 963 K. New high-temperature single-crystal X-ray diffraction experiments at 1100 K revealed that $Ca_2Fe_2O_5$ forms an incommensurately modulated structure adopting the superspace group $Imma(00\gamma)s00$, with $\gamma = 0.588\,(2)$. The modulation affects the sequence of the enantiomorphic (right- and left-handed) oriented tetrahedral chains within the layer, breaking the lattice periodicity along **c**. This ordering can be modelled with crenel occupation modulation functions for the tetrahedrally coordinated Fe, as well as for the O atom interconnecting the tetrahedra.

1. Introduction

Since the early investigations of Hansen *et al.* (1928) on the ternary system $CaO–Al_2O_3–Fe_2O_3$, the solid-solution series $Ca_2(Fe_{1-x}Al_x)_2O_5$ has been the subject of many phase analytical, magnetic and structural studies (Bertaut *et al.*, 1959; Smith, 1962; Tarte, 1964, 1965*a*,*b*; Pobell & Wittmann, 1965; Geller *et al.*, 1970; Colville & Geller, 1971; Geller *et al.*, 1971; Berggren, 1971; Colville & Geller, 1972; Zeng & Yang, 1991; Kim *et al.*, 1995; Kahlenberg & Fischer, 2000; Redhammer *et al.*, 2004). This interest is mainly due to the fact that Ca_2FeAlO_5 (brownmillerite) is one of the four major phases in Portland cement clinkers. According to Taylor (1997), the solid-solution series exists at ordinary pressures in the compositional range between $x = 0$ and $x = 0.7$. From a structural point of view, two different space-group types have to be distinguished. The pure iron end member (mineral name srebrodolskite) as well as the compositions up to x of about 0.28 adopt the space group *Pnma*, whereas the samples beyond $x = 0.28$ crystallize in the space group *I*2*mb*. The pure Al end member can be obtained only at elevated pressure (Kahlenberg *et al.*, 2000). The basic building elements of the two modifications are the same, involving (*a*) layers of perovskite-type corner-sharing $(Fe,Al)O_6$ octahedra and (*b*) so-called *zweier* single chains (Liebau, 1985) of $(Fe,Al)O_4$ tetrahedra. Fig. 1 shows the *Pnma* brownmillerite-type structure of $Ca_2Fe_2O_5$. The octahedral layer is depicted in light grey, the tetrahedral chains are dark grey. The alternate stacking of the octahedral layers and the sheets of single chains forms a three-dimensional network in which the Ca

cations are located for charge compensation. They are coordinated by eight O atoms. The basic difference between the two modifications results from different orientations of the tetrahedral chains in *Pnma* as opposed to only one in *I*2*mb*. The first evidence for additional structural changes in dicalcium ferrate at elevated temperatures was given by Woermann *et al.* (1968). In DTA experiments, they observed two weak reversible thermal effects occurring at 703 and 963 K, respectively. Magnetic measurements based on ^{57}Fe Mössbauer spectroscopy and neutron diffraction (Takeda *et al.*, 1968) revealed that $Ca_2Fe_2O_5$ is an antiferromagnet and that the first thermal effect corresponds to the Néel temperature of the material. No additional structural changes were observed. For the temperature region above the second transition, contradictory results have been reported. Whereas Shin *et al.* (1979) proposed that $Ca_2Fe_2O_5$ still belongs to *Pnma* up to 1373 K, a high-temperature powder X-ray diffraction study by Kahlenberg *et al.* (1998) pointed to a phase transition at T_c = 961 K from an orthorhombic primitive to a body-centred Bravais lattice. It was suggested that the high-temperature (HT) modification may adopt the *I*2*mb* structure type that is realized for the Al-containing phases at room conditions. According to a Rietveld analysis based on neutron diffraction on polycrystalline samples performed by Berastegui *et al.* (1999), $Ca_2Fe_2O_5$ can be described in the space group *Imma*, indicating a disorder of the tetrahedra. In the course of an ongoing research project on alkaline-earth ferrates, we re-investigated the structural phase transition in $Ca_2Fe_2O_5$ using high-temperature single-crystal X-ray diffraction. The diffraction experiments revealed that the HT modification is considerably more complex than suggested by Berastegui *et al.* (1999). We found that above T_c an incommensurately modulated structure is formed. The present paper describes the crystal structure of the incommensurately modulated HT phase of $Ca_2Fe_2O_5$ in detail, and also compares this structure to the known commensurate brownmillerite-type phases investigated by Lambert *et al.* (2002) and Abakumov *et al.* (2003). Structural reasons for the ordering of the tetrahedral chains as proposed by Abakumov *et al.* (2005) will be discussed.

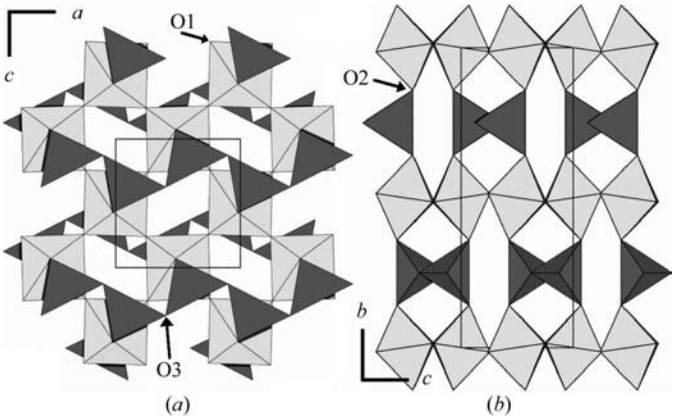

Figure 1
The brownmillerite-type structure of $Ca_2Fe_2O_5$ in *Pnma*. Ca atoms have been omitted for clarity. Projection along (*a*) [010] and (*b*) [100].

Table 1
Experimental details.

Crystal data	
Chemical formula	$Ca_2Fe_2O_5$
M_r	271.8
Cell setting, superspace group	Orthorhombic, *Imma*(00γ)*s*00 (No. 74.2)
a, *b*, *c* (Å)	5.4931 (12), 15.038 (3), 5.6511 (11)
V (Å^3)	466.79 (17)
Z	4
D_x (Mg m^{-3})	3.867
Radiation type	Mo $K\alpha$
No. of reflections for cell parameters	2473
θ range (°)	2.7–29.5
μ (mm^{-1})	8.33
Temperature (K)	1100
Crystal form, colour	Plate, reddish-brown
Crystal size (mm)	0.18 × 0.18 × 0.06
Data collection	
Diffractometer	Stoe IPDS-2
Data collection method	Rotation method
Absorption correction	Integration
T_{min}	0.309
T_{max}	0.609
No. of measured, independent and observed reflections	6040, 934, 759
Criterion for observed reflections	$I > 3\sigma(I)$
R_{int}	0.059
θ_{max} (°)	29.3
Range of *h*, *k*, *l*	$-7 \Rightarrow h \Rightarrow 7$ $-20 \Rightarrow k \Rightarrow 20$ $-7 \Rightarrow l \Rightarrow 7$ $-1 \Rightarrow m \Rightarrow 1$
Refinement	
Refinement on	*F*
$R[F^2 > 2\sigma(F^2)]$, $wR(F^2)$, *S*	0.053, 0.055, 2.91
No. of reflections	934
No. of parameters	43
Weighting scheme	Based on measured s.u.'s; $w = 1/[\sigma^2(F) + 0.0001F^2]$
$(\Delta/\sigma)_{max}$	0.001
$\Delta\rho_{max}$, $\Delta\rho_{min}$ (e Å^{-3})	1.29, −1.96

Computer programs used: *Stoe X-AREA* (Stoe & Cie GmbH, 2005), *Stoe X-RED*, *JANA*2000 (Petříček *et al.*, 2000).

2. Experimental

2.1. Synthesis

For single-crystal growth of $Ca_2Fe_2O_5$, the flux technique was applied. Growth experiments were performed with calcium chloride as a high-temperature solvent. The starting materials were $CaCO_3$ (Merck, 99%) as well as Fe_2O_3 (Fluka, 99.9%). The reagents were carefully mixed in an agate mortar. Dried $CaCl_2$ (Merck, purum) was added and the compounds were mixed again. A sample of 4 g with a nutrient-to-flux ratio of 1:3 was placed in a 50 ml platinum crucible with a crimped platinum cover. The mixture was heated from 373 to 1323 K over a period of 11 h in a resistance-heated furnace; it was held at this temperature for 6 h in order to homogenize the melt, then cooled down to 1173 K at a rate of 5 K h^{-1} and quenched immediately. The reddish-brown crystals were concentrated at the bottom of the crucible and could easily be removed from the matrix of solidified flux by hand. The obtained samples showed well developed external faces of the

{010}, {101} and {110} forms, exhibiting edges up to 2 mm in length and habits ranging from platy to lath-shaped.

2.2. X-ray data collection

A suitable crystal of platy shape was selected using a polarizing microscope. The crystal was fixed in the constricting part of a 0.1 mm quartz-glass capillary. X-ray diffraction data collection was performed with a two-circle Stoe IPDS-2 imaging-plate diffractometer. A nitrogen heat-stream furnace was used to heat the crystal for HT data collection. The device was mounted on the ω axis in such a way that the outlet of the hot N_2 stream was placed 3.25 mm underneath the sample for all goniometer positions. The stability of the temperature was achieved using a digital gas-flow meter, keeping the stream of N_2 constant and by means of a highly stabilized power unit. The data were collected at 1100 K and were subsequently analytically corrected for absorption using eight indexed faces. Corrections for Lorentz, polarization and air absorption effects were applied. Further details of the data collection are summarized in Table 1.

2.3. Refinement

The X-ray diffraction experiment at 1100 K basically confirmed the *I*-centred cell, which was reported earlier by Berastegui *et al.* (1999). However, only about 50% of the peaks found in the diffraction pattern could be indexed with this cell, using an *hkl* index tolerance of 0.2. Therefore, reciprocal space was reconstructed from the imaging-plate data. Precession-type oriented sections revealed the incommensurate nature of the HT phase. The (1*kl*) section (Fig. 2), for example, shows additional reflections with non-integer values for *l*. The satellites can be indexed with a **q** vector of $(0,0,\gamma)$ (de Wolff, 1974), assigning them to the next non-extinct main reflection along $\mathbf{c}^*$. γ was refined to 0.588 (2) using the **q**-vector tool of the *X-AREA* software (Stoe & Cie GmbH, 2005). Subsequently, the data were integrated including satellite reflections of first order. Second-order reflections were not observed. The systematic extinction of the 0*klm* reflections with $m \neq 2n$ indicates the presence of a glide plane with a glide vector in the internal space. Since only first-order satellite reflections were observed, no satellites can be seen in the section (0*klm*) (Fig. 3). Assuming *Imma* to be the space group of the average structure, this leads to *Imma*(00γ)*s*00 (No. 74.2) as the (3 + 1)-dimensional superspace group (Janssen *et al.*, 1995). The superspace group *Imma*(00γ)*ss*0 (No. 74.3) could be excluded because the required extinction condition *h*0*lm*: $m \neq 2n$ is not fulfilled. Alternatively, the equivalent less-common superspace group *Xmma*(00γ)*s*00, with a centring vector of $(\frac{1}{2},\frac{1}{2},\frac{1}{2},\frac{1}{2})$, could be used by assigning the satellites to the extinct main reflections. Therefore, the γ compound of the **q** vector has to be transformed to $1-\gamma$. However, we decided to use the standard setting *Imma*(00γ)*s*00.

A (3 + 1)-dimensional structural model describing the ordering of tetrahedral chains in brownmillerites was first introduced by Lambert *et al.* (2002) for commensurate phases of the $Ca_2Co_{2-x}Al_xO_5$ system. This model is now adopted for incommensurate $Ca_2Fe_2O_5$.

The structure refinements were carried out using the computer program *JANA*2000 (Petříček *et al.*, 2000). Additional information concerning the refinement is listed in Table 1. Taking into account the main reflections only, a reasonable fit of R_{obs} = 0.046 was reached using Berastegui *et al.*'s (1999) three-dimensional structural model.

In the *Imma* model of the average structure, the tetrahedral chains are disordered. The tetrahedrally coordinated Fe2 atom is modelled as a split atom, as well as the O3 atom – which is the atom connecting the tetrahedra along the chain – and its

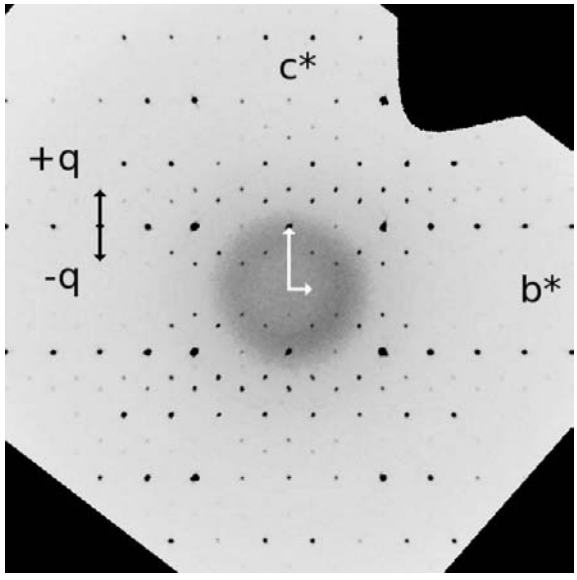

Figure 2
Reciprocal-space section (1*kl*), calculated from imaging-plate data. Satellite reflections and the corresponding **q** vector are shown.

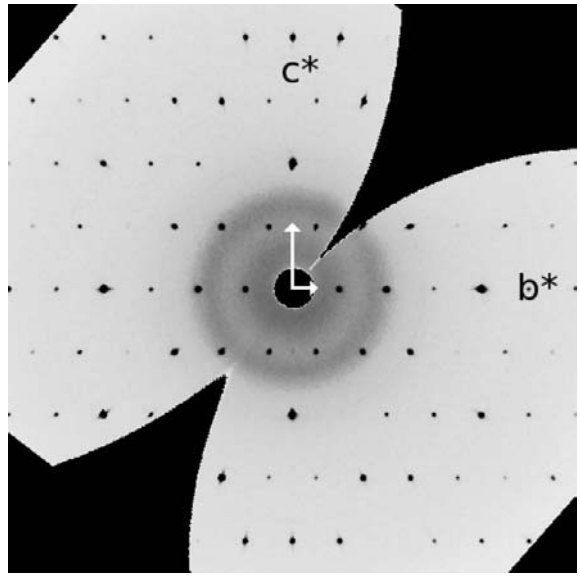

Figure 3
Reciprocal-space section (0*kl*), calculated from imaging-plate data. Satellite reflections are systematically absent.

equivalent. The vertices connecting to the octahedral layers (O2) are not affected by the disorder. The atoms Fe2 and O3 are doubled by the mirror plane m_a resulting in two alternative orientations of the tetrahedra. The resulting *zweier* single chains exist in two enantiomorphic orientations, which will be arbitrarily called L (left) and R (right).

If the orientation of the chain is subject to the modulation, it should be a periodic function in x_4. Each of the two atoms (Fe2 and O3) defining the orientation of the chains can adopt two distinct x_1 positions, which are symmetry equivalent by a super glide plane ${}^{m_a}_{s}$ with an intrinsic shift of $\tau = \frac{1}{2}$. Since the equivalent sites of these atoms are linked by the intrinsic shift of $\frac{1}{2}$, it is sufficient to model each atom with a crenel-type occupation modulation function (Petříček *et al.*, 1995). To describe a crenel function, only two parameters are needed. x_4^0, which represents the centre of the crenel function in x_4, and the width of the 'crenels', Δ. The crenel function can only adopt values of 0 or 1. For x_4 coordinates in the interval $x_4^0 \pm \Delta/2$, the function is equal to 1 and in any other case 0. If crenel-type occupation modulation functions with a width of $\Delta = \frac{1}{2}$ are used, only one of the equivalent atoms is present for any value of x_4. The effect of the crenel functions can be seen in the $x_1 - x_4$ sections of the four-dimensional $F_{\rm obs}$ Fourier synthesis of the Fe2 and O3 atom environments (Figs. 4 and 5). Both atoms are switching between their symmetry-equivalent x_1 coordinates as a function of x_4. Since Fe2 and O3 atoms belong to differently oriented tetrahedra, they are not allowed to exist simultaneously within one cell for any physical space section. The phases of their crenel functions have to be shifted by $\frac{1}{2}$, which requires the following equation to be fulfilled.

$$x_4^0(\mathrm{O3}) + \tfrac{1}{2} - \gamma x_3^0(\mathrm{O3}) = x_4^0(\mathrm{Fe2}) - \gamma x_3^0(\mathrm{Fe2}).$$

x_4^0 represents the centre of the crenel function in x_4 and x_3^0 the z coordinate of the given atom in the basic structure. Although this equation was not used to constrain the refinement, it was fulfilled within the errors given by the refinement. Combining the crenel-type modulated atoms with additional positional modulations did not significantly improve the refinement.

All other atoms can be modelled with harmonic positional modulation functions. The sine and cosine terms of the first harmonic wave of the modulation functions were refined, where not restricted by symmetry. Additionally, anisotropic temperature factors were refined for all atoms. Modulation of the temperature factors was tried, but led to negative temperature parameters and was therefore discounted.[1]

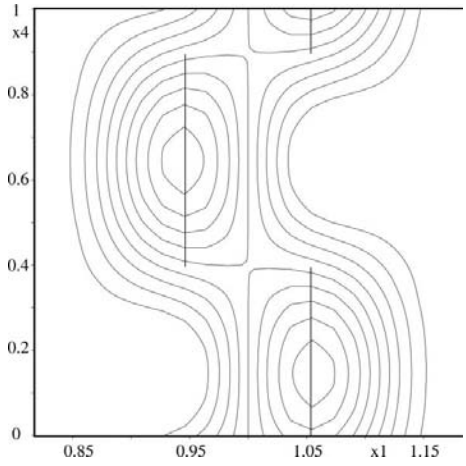

Figure 4
The crenel-function modulation of the Fe2 atom. $x_1 - x_4$ map, intersecting the four-dimensional $F_{\rm obs}$ Fourier synthesis at $x_2 = 0.25$, $x_3 = 0.569$. Contour lines from 10 to 90 e Å^{-3} in intervals of 10 e Å^{-3}.

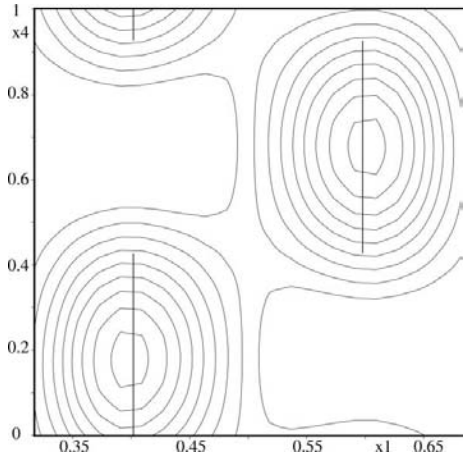

Figure 5
The crenel-function modulation of the O3 atom. $x_1 - x_4$ map, intersecting the four-dimensional $F_{\rm obs}$ Fourier synthesis at $x_2 = 0.25$, $x_3 = 0.626$. Contour lines from 2 to 18 e Å^{-3} in intervals of 2 e Å^{-3}.

Table 2
Interatomic distances including averages (ave) and extrema caused by the modulation.

	$d_{\rm ave}$ (Å)	$d_{\rm min}$ (Å)	$d_{\rm max}$ (Å)	Symmetry codes
Fe1—O1	1.980 (2)	1.9676 (8)	1.9927 (8)	(i), (ii), (iii), (iv)
Fe1—O2	2.162 (4)	2.160 (4)	2.163 (4)	(v), (vi)
Fe2—O2	1.844 (4)	1.828 (4)	1.852 (4)	(vii), (viii)
Fe2—O3	1.919 (5)	–	–	(ix)
Fe2—O3	1.941 (4)	–	–	(iii)
Ca1—O1	2.514 (4)	2.485 (3)	2.543 (3)	(x), (xi)
Ca1—O1	2.616 (4)	2.581 (3)	2.652 (3)	(iv), (xii)
Ca1—O2	2.360 (4)	2.359 (4)	2.360 (4)	(v)
Ca1—O2	2.803 (5)	2.622 (5)	2.984 (5)	(xii), (xiv)
Ca1—O3	2.369 (2)	2.356 (2)	2.376 (2)	(xv), (xvi)

Symmetry codes: (i) $-1+x, y, z$; (ii) $1-x, -y, 1-z$; (iii) $1-x, y, z$; (iv) $-1+x, -y, 1-z$; (v) x, y, z; (vi) $-x, -y, 1-z$; (vii) $1+x, y, z$; (viii) $1+x, \frac{1}{2}-y, z$; (ix) $\frac{3}{2}-x, \frac{1}{2}-y, \frac{3}{2}-z$; (x) $1-x, y, -1+z$; (xi) $-1+x, y, -1+z$; (xii) $1-x, -y, 1-z$; (xii) $\frac{1}{2}-x, y, \frac{1}{2}-z$; (xiv) $-\frac{1}{2}-x, y, \frac{1}{2}-z$; (xv) $-\frac{1}{2}+x, \frac{1}{2}-y, \frac{1}{2}-z$; (xvi) $\frac{1}{2}-x, \frac{1}{2}-y, \frac{1}{2}-z$.

3. Modulated structure

The resulting aperiodic order of the tetrahedral chains can be seen in the physical-space section at $x_2 = 0.25$, intersecting the tetrahedral layers in O3 and Fe2 atoms. The corresponding map has been calculated from four-dimensional $F_{\rm obs}$ Fourier synthesis for $t = 0$ (Fig. 6). There is no periodicity in the sequence of L or R chains along x_3. For the chains at

[1] Supplementary data for this paper, including atomic coordinates, anisotropic displacement parameters and coefficients of the modulation functions, are available from the IUCr electronic archives (Reference: SN5023). Services for accessing these data are described at the back of the journal.

$x_3 \simeq 1, 2, 7, 8$, the maxima in the electron density corresponding to the atoms Fe2 and O3 are elongated or show additional maxima, respectively. This is due to termination effects of the Fourier synthesis, as can be seen in the overlapping of electron density in the $x_1 - x_4$ sections of Fe2 and O3 atoms (Figs. 4 and 5).

Ca1 and O2 are the only atoms exhibiting a significant displacive modulation, which is illustrated in a displacement plot (Fig. 7). The maximum absolute displacement as shown by the O2 atom is *ca* 0.6 Å. The modulation functions of Ca1 and O2 atoms are more or less 'in phase' (see Fig. 7), therefore the Ca1—O2 distance (see Table 2) is not much affected by the modulations.

The two symmetry-equivalent atoms of O2 coordinating the Ca1 atom are phase shifted in a way such that their displacements are in the opposite direction of the displacements of the Ca1 atom (Fig. 7). This causes variations of up to 0.36 Å in their distances to the Ca1 atom (Table 2). Nevertheless, the bond-valence sum (Brown & Altermatt, 1985) for the Ca1 atom is not seriously influenced by the modulation, as can be seen in Table 3. A closer look at the octahedra reveals that the x_1 modulation of the O2 atom (connecting octahedra and tetrahedra) results in a rotation of the O2—O2 axis of the octahedra around [001]. Interestingly, this does not cause a significant variation in the O2—O2 distances within the tetrahedral chains. The displacement plot (Fig. 8) of three equivalent O2 atoms having the same x_2 shows that the O2 atom in (x_1, x_2, x_3) and the O2 atom in $(x_1 + \frac{1}{2}, x_2, \frac{5}{4} - x_3)$ (which belong to one tetrahedral chain) move 'in phase'. Therefore, no significant variations in the distance result. The modulation of the O2 atom in $(x_1 + \frac{1}{2}, x_2, \frac{1}{4} - x_3)$ (which belongs to the neighbouring tetrahedral chains) is phase shifted against the O2 atom in (x_1, x_2, x_3), resulting in larger fluctuations of the distances. This is because the O2—O2 distance in x_3 is bigger within the tetrahedral chains than the corresponding O2—O2 separation from neighbouring tetrahedral chains. Hence, the phase shift is different.

Table 3
Bond-valence sums, including averages (ave) and extrema caused by the modulation.

Atom	BVS_{ave}	BVS_{min}	BVS_{max}
Fe1	2.87 (5)	2.87 (5)	2.88 (5)
Fe2	2.854 (16)	2.817 (16)	2.915 (16)
Ca1	1.708 (7)	1.701 (6)	1.715 (7)

4. Discussion

Superstructures in brownmillerite-type compounds have been observed frequently, *e.g.* in Sr_2MnGaO_5 (Abakumov *et al.*,

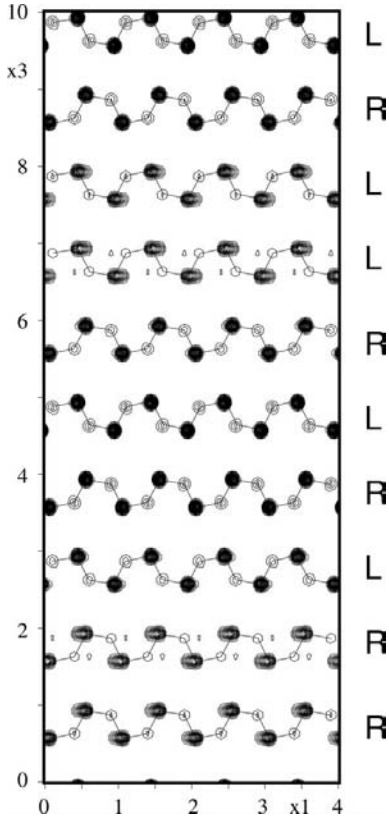

Figure 6
Physical-space map $(x_1 - x_3)$ at $t = 0$, $x_2 = 0.25$ calculated from four-dimensional F_{obs} Fourier synthesis. The incommensurately modulated sequence of right- (R) and left-handed (L) tetrahedral chains can be seen.

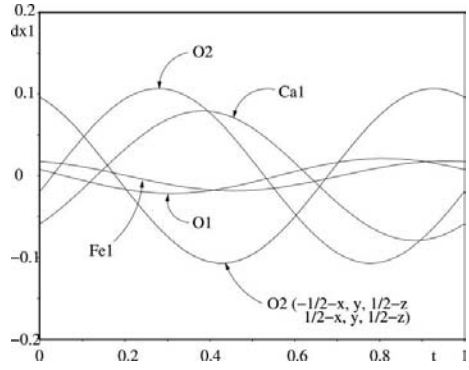

Figure 7
Displacement in x_1 of Ca1, O2, O1, Fe1 atoms as a function of *t*.

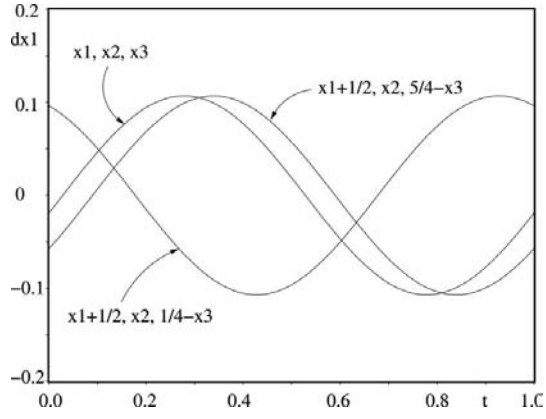

Figure 8
Displacement of three neighbouring O2 atoms as a function of *t*.

2001), Sr_2CuGaO_5 (Ruiz-González *et al.*, 2002) and $Ca_2Co_{2-x}Al_xO_5$ (Lambert *et al.*, 2002). These superstructures have different sequences of R- and L-oriented chains within the tetrahedral layers. Two of these compounds have already been described with the superspace formalism: Lambert *et al.* (2002) found a commensurately modulated (3 + 1)-dimensional model for $Ca_2Co_{2-x}Al_xO_5$. For compositions close to $x = 0.75$, they reported modulation wavevector compounds α (which corresponds to γ in the *Imma* setting) of $\frac{1}{2}$, $\frac{5}{8}$, $\frac{2}{3}$ and $\frac{7}{9}$ found by electron diffraction. They performed X-ray diffraction experiments on two crystals with α of $\frac{5}{8}$ and $\frac{2}{3}$. (All **q** vectors are oriented within the tetrahedral layer, perpendicular to the direction of the chains, which corresponds to the *c* direction in the *Imma* setting.) According to their findings, the octahedral position is preferentially occupied by Co atoms (84%), whereas the tetrahedral site shows a more equal distribution of Co atoms ($\sim$ 40%) and Al atoms ($\sim$ 60%). Abakumov *et al.* (2003) found **q** vectors $(0, 0, \gamma)$ with γ of $\frac{1}{2}$ and $\frac{2}{5}$ in Sr_2MnGaO_5. They also described that compound in (3 + 1)-dimensional superspace. Sr_2MnGaO_5 shows a strict ordering of Mn (octahedral sites) and Ga (tetrahedral sites) atoms. However, unlike the HT phase of $Ca_2Fe_2O_5$, these compounds are commensurate structures, with two different *B* cations, which are either ordered or disordered over the tetrahedral and octahedral positions.

In a recently published paper by Abakumov *et al.* (2005), a compositionally induced phase transition in the solid-solution series of $Ca_2MnGa_{1-x}Al_xO_5$ is investigated. Two competing mechanisms are described as the driving forces for tetrahedral chain ordering. It is shown that each tetrahedral chain is associated with an electric dipole moment. These dipole moments are oriented along the chain directions and have opposite signs for R- and L-type chains. In order to minimize the free energy caused by the dipole–dipole interactions, the tetrahedral chains should tend to an alternate ordering (LRLR) within one layer. This corresponds to a commensurate *Imma*$(00\gamma)s00$ structure with $\mathbf{q} = \frac{1}{2}\mathbf{c}^*$ (Abakumov *et al.*, 2003). The *Pnma* symmetry (as found in $Ca_2Fe_2O_5$ at ambient conditions) exhibits only one type of chain in each tetrahedral layer, whereas the layers show alternate stacking of R and L layers. The compensation of the dipole moments in this arrangement (alternating layers) is less favourable than in the arrangement of alternating chains. In the case of *I*2*mb* symmetry, there is only one type of chain. The dipole moments are not compensated at all.

The competing mechanism is the distortion of the adjacent octahedral layers, induced by the sequence of chains in the tetrahedral layer. Abakumov *et al.* (2005) studied the displacement of the O2 atom from its position in the undistorted perovskite structure. In all types of brownmillerite structures, the O2 atom – connecting octahedral and tetrahedral layers – is shifted along [001]. Therefore, octahedra are rotated around [100]. This results in alternate tilted octahedra, as can be seen in Fig. 1(*b*). If alternating R- and L-type chains are present within one layer, a distortion of the octahedra will be induced. The O2 atom is shifted along [100] in opposite directions for chains of different types. A rotation around [001] in the same direction is not possible for two adjacent octahedra connected to the same tetrahedral chain (see Fig. 11 in Abakumov *et al.*, 2005).

According to the results of Abakumov *et al.* (2005), a change in the strength of the dipole moments is reflected by a change of the $T-O3-T$ angles. For larger deviations of this angle from 180°, the resulting dipole moment increases. They report about 121° for Ca_2MnGaO_5 and approximately 142° for Ca_2MnAlO_5. For $Ca_2Fe_2O_5$, we calculated the corresponding angles as a function of the temperature from the structural data given by Berastegui *et al.* (1999). However, no significant changes could be detected [125.7 (1)° at room conditions, 126.1 (3)° at 1273 K]. Therefore, a change in the strength of the dipole moments can be excluded as a driving force of the transition to the modulated sequence of R and L chains within the tetrahedral layers.

From temperature-dependent bond-valance calculations, Berastegui *et al.* (1999) concluded that the Fe2—O bonds (tetrahedra) are highly covalent in contrast to the longer Fe1—O bonds (octahedra). This effect results in an anisotropic thermal expansion of this compound. The tetrahedral layers are constraining the expansion in the (010) plane. The relative thermal expansion in the range from room conditions to 1273 K is *ca* 1.9% for the *b* direction and approximately 1% for *a* and *c*. We calculated the O2—O2 distances for the octahedra as well as for the tetrahedra from Berastegui *et al.* (1999) structural data to reveal the thermal expansion along [010] of these structural units. The relative thermal expansion of the octahedral and tetrahedral layers along the *b* direction is *ca* 1.8 and 0.4%, respectively (from room conditions to 1273 K). During the thermal expansion of the structure, the distances between the tetrahedral layers increase disproportionally more compared with the rest of the structure. With increasing distance between the tetrahedral layers, it becomes energetically more reasonable to compensate the dipole moments within the layers. The aperiodic order of the sequence of tetrahedral chains can be assumed to minimize the structural distortions, which would be induced by a strictly alternating sequence.

The authors are grateful to the Co-editor, Sander van Smaalen, and the referees, whose valuable comments improved the paper. We also wish to thank Václav Petříček for some helpful discussion, as well as for his instant answers to any questions concerning the software *JANA*2000.

References

Abakumov, A. M., Alekseeva, A. M., Rozova, M. G., Antipov, E. V., Lebedev, O. I. & Van Tendeloo, G. (2003). *J. Solid State Chem.* **174**, 319–328.

Abakumov, A. M., Kalyuzhnaya, A. S., Rozova, M. G., Antipov, E. V., Hadermann, J. & Van Tendeloo, G. (2005). *Solid State Sci.* **7**, 801–811.

Abakumov, A. M., Rozova, M. G., Pavlyuk, B. P., Lobanov, M. V., Antipov, E. V., Lebedev, O. I., Van Tendeloo, G., Ignatchik, O. L.,

Ovtchenkov, E. A., Koksharov, Y. A. & Vasil'ev, A. N. (2001). *J. Solid State Chem.* **160**, 353–361.
Berastegui, P., Eriksson, S.-G. & Hull, S. (1999). *Mater. Res. Bull.* **34**, 303–314.
Berggren, J. (1971). *Acta Chem. Scand.* **25**, 3616–3624.
Bertaut, E. F., Blum, P. & Sagnières, A. (1959). *Acta Cryst.* **12**, 149–159.
Brown, I. D. & Altermatt, D. (1985). *Acta Cryst.* B**41**, 244–247.
Colville, A. A. & Geller, S. (1971). *Acta Cryst.* B**27**, 2311–2315.
Colville, A. A. & Geller, S. (1972). *Acta Cryst.* B**28**, 3196–3200.
Geller, S., Grant, R. W. & Fullmer, L. D. (1970). *J. Phys. Chem. Solids*, **31**, 793–803.
Geller, S., Grant, R. W. & Gonser, U. (1971). *Prog. Solid State Chem.* **5**, 1–26.
Hansen, W. C., Brownmiller, L. T. & Bogue, R. H. (1928). *J. Am. Chem. Soc.* **50**, 396–406.
Janssen, T., Janner, A., Looijenga-Vos, A. & de Wolff, P. M. (1995). *International Tables for Crystallography*, Vol. C, ch. 9.8. Dordrecht: Kluwer Academic Publishers.
Kahlenberg, V. & Fischer, R. X. (2000). *Eur. J. Mineral.* **12**, 129–135.
Kahlenberg, V., Fischer, R. X. & Shaw, C. S. J. (2000). *Am. Mineral.* **85**, 1061–1065.
Kahlenberg, V., Fischer, R. X., Weidenthaler, C. & Zeiske, T. (1998). 17th General Meeting of the International Mineralogical Association, Toronto.
Kim, G. Y., Roh, K. S. & Yo, C. H. (1995). *Bull. Korean Chem. Soc.* **16**, 934–938.
Lambert, S., Leligny, H., Grebille, D., Pelloquin, D. & Raveau, B. (2002). *Chem. Mater.* **14**, 1818–1826.
Liebau, F. (1985). *Structural Chemistry of Silicates – Structure, Bonding, and Classification.* Berlin: Springer-Verlag.
Petříček, V., Dušek, M. & Palatinus, L. (2000). *JANA*2000. Institute of Physics, Praha, Czech Republic.
Petříček, V., van der Lee, A. & Evain, M. (1995). *Acta Cryst.* A**51**, 529–535.
Pobell, F. & Wittmann, F. (1965). *Phys. Lett*. **19**, 175–176.
Redhammer, G. J., Tippelt, G., Roth, G. & Amthauer, G. (2004). *Am. Mineral.* **89**, 405–420.
Ruiz-González, M. L., Prieto, C., Alonso, J., Ramírez-Castellanos, J. & González-Calbet, J. M. (2002). *Chem. Mater.* **14**, 2055–2062.
Shin, S., Yonemura, M. & Ikawa, H. (1979). *Bull. Chem. Soc. Jpn*, **52**, 947–948.
Smith, D. (1962). *Acta Cryst.* **15**, 1146–1152.
Stoe & Cie GmbH (2005). *X-AREA*. Darmstadt, Germany.
Takeda, T., Yamaguchi, Y., Tomiyoshi, S., Fukase, M., Sugimoto, M. & Watanabe, H. (1968). *J. Phys. Soc. Jpn*, **24**, 446–452.
Tarte, P. (1964). *Rev. Chim. Mineral.* **1**, 425–438.
Tarte, P. (1965*a*). *Silicates Ind*. **31**, 343–352.
Tarte, P. (1965*b*). *Nature (London)*, **207**, 973–974.
Taylor, H. F. W. (1997). *Cement Chemistry*, 2nd ed. London: Thomas Telford.
Woermann, W., Eysel, W. & Hahn, T. (1968). *Proc. 5th Int. Symp. Chem. Cem.* **I**, 54–60.
Wolff, P. M. de (1974). *Acta Cryst.* A**30**, 777–785.
Zeng, Y. & Yang, N. (1991). *Cem. Concr. Res.* **21**, 31–37.